International Journal of Nanomedicine

Dovepress

open access to scientific and medical research

Open Access Full Text Article

ORIGINAL RESEARCH

Cucumber-Derived Nanovesicles Containing Cucurbitacin B for Non-Small Cell Lung Cancer Therapy

Tingting Chen[1,2,*], Bingxiang Ma[1,2,*], Shi Lu[1,2], Lupeng Zeng[1,2], Huaying Wang[1,2], Wanhua Shi[1,2], Linying Zhou[3], Yaokun Xia[4], Xi Zhang[1], Jing Zhang[5], Jinghua Chen[1]

[1]School of Pharmacy, Fujian Medical University, Fuzhou, Fujian Province, 350108, People's Republic of China; [2]Fujian Key Laboratory of Drug Target Discovery and Structural and Functional Research, Fujian Medical University, Fuzhou, Fujian Province, 350108, People's Republic of China; [3]Electron Microscopy Facility, Public Technology Service Center, Fujian Medical University, Fuzhou, Fujian Province, 350108, People's Republic of China; [4]Key Laboratory of the Ministry of Education for Gastrointestinal Cancer, School of Basic Medical Sciences, Fujian Medical University, Fuzhou, Fujian Province, 350108, People's Republic of China; [5]Department of Chemical Biology, College of Life Sciences, Fujian Agriculture and Forestry University, Fuzhou, Fujian Province, 350002, People's Republic of China

*These authors contributed equally to this work

Correspondence: Jinghua Chen, School of Pharmacy, Fujian Medical University, Fuzhou, Fujian Province, 350108, People's Republic of China, Tel +86 591-22862016, Fax +86 591-22862016, Email cjh_huaxue@126.com; xz@fjmu.edu.cn

Purpose: In recent years, a variety of nanoparticles with excellent anticancer and delivery properties have emerged for cancer therapy. However, potential toxicity, high production cost and complex preparation procedures have been obstacles to their use in biomedicine. Here, we obtained cucumber-derived nanovesicles (CDNVs) at high yield and low cost by simple juicing and ultracentrifugation. The anticancer effects of CDNVs were evaluated in vitro and in vivo.

Methods: Transmission electron microscope, nanoparticle tracking analysis and laser particle size analysis were used to characterize the morphology, diameter and zeta potential of CDNVs, respectively. The anticancer effects of CDNVs in vitro were evaluated by MTT and apoptosis assays. The mechanism was further explored by measuring the protein levels of signal transducer and activator of transcription 3 pathway, reactive oxygen species, cell cycle distribution and caspase activity. In-vivo anticancer efficacy was evaluated by measuring tumor volume and weight of mice in three different treatment groups (CDNVs, cucurbitacin B and PBS).

Results: CDNVs inhibited proliferation of human non-small cell lung cancer cells by suppressing signal transducer and activator of transcription 3 activation, generating reactive oxygen species, promoting cell cycle arrest, and activating the caspase pathway. These CDNVs exhibited strong anticancer effects both in vitro and in vivo, and reduced the rate of tumor growth without obvious toxicity to mouse visceral organs. Compared with an equivalent dose of cucurbitacin B, CDNVs exerted stronger anticancer effects in vitro and in vivo.

Conclusion: These results demonstrate that CDNVs suppress tumor growth. This study addresses the development of cancer therapeutic drugs using plant-derived nanovesicles that are cost-efficient, simple to produce in high yields, and provide an alternative approach to drug isolation that may help advance sustainability of medicinal plants.

Keywords: ROS, STAT3, cucurbitacin B, anticancer

Introduction

As a life-threatening disease, cancer is of major public health and economic concern worldwide.[1–4] Different treatment strategies have been widely explored in cancer therapy, including chemotherapy and photothermal, photodynamic, and gene therapy.[5–7] In these strategies, therapeutic agents are typically bound to or encapsulated in nanocarriers such as exosomes, liposomes, micelles, and inorganic, DNA and protein nanoparticles,[8–13] for efficient delivery to tumors in vivo. Regardless of the value of these nanocarriers for drug delivery, the complex manufacturing processes required for synthetic nanocarriers limit the scale of production, and potential in-vivo toxicity remains a challenge to their clinical use. Hence, there remains an urgent need to develop simple, safe, and effective drug delivery systems.

Received: 25 February 2022
Accepted: 28 July 2022
Published: 10 August 2022

Currently, increased attention is being given to development of green, sustainable and biocompatible materials for delivery of bioactive compounds for pharmaceutical and medical applications. The potential of plant-derived nanovesicles (PDNVs) as safe nanocarriers for drug delivery has been demonstrated in recent studies in which simple preparation procedures were described.[14,15] PDNVs typically exist in roots, stems, leaves and fruits of plants, and are involved in plant cell communication.[16,17] PDNVs have several potential advantages as nanocarriers. Firstly, they can be efficiently obtained and thus offer the possibility of large-scale production.[18,19] Secondly, PDNVs have cross-kingdom effects.[20,21] Thirdly, PDNVs can pass through the blood-brain barrier without crossing the placental barrier, so they can deliver drugs for brain diseases, such as Parkinson's disease and stroke, without impacting the fetus.[22] Fourthly, PDNVs may possess inherent targeting characteristics and display affinity toward particular tissues.[23] Also, PDNV structure is usually minimally affected by loading, and their high biocompatibility supports drug delivery and efficacy.[24] Thus, PDNVs have been exploited as excellent candidates for encapsulation of chemotherapeutic drugs, RNAs, proteins, and other therapeutic anticancer agents.[24–26]

Another important feature of PDNVs is that they contain intrinsic bioactive compounds that may help boost their anticancer effects, making them even more appealing. For example, Özkan et al found that garlic-derived nanovesicles (GaDNVs) induce apoptosis by activating intrinsic pathways without having been loaded with therapeutic drugs,[27] suggesting that bioactive compounds in GaDNVs have anticancer effects. However, most studies have not identified the bioactive molecules that endow PDNVs with such anticancer effects, let alone compared the anticancer effects of free and encapsulated bioactive molecules.[28,29] Without that information, it is difficult to usefully discuss the advantages of PDNVs in anticancer research.

Cucurbitacin B (CuB), a tetracyclic triterpenoid molecule, has been reported to inhibit development of leukemia, breast cancer, lung cancer and hepatoma.[30–33] However, satisfactory anticancer activity often requires a large dose of CuB because of its low solubility and bioavailability.[34,35] To overcome this limitation, Bakar-Ates et al and Tang et al utilized nanocarriers, lipid polymer hybrid nanocarriers and nanomicelles, to load CuB, and both exhibited greater cytotoxicity than free CuB.[35,36] But the limitations of synthetic nanocarriers, like complex preparation and potential in-vivo toxicity, limit their use as mentioned above.

As a member of the Cucurbitaceae family of plants, cucumbers contain CuB. Thus, we reasoned that cucumber-derived nanovesicles (CDNVs) could be natural nanocarriers that contain CuB and can exert native anticancer activity against various cancers without requiring extraction and loading of CuB. As shown in Scheme 1, we isolated CDNVs using simple juicing and centrifugation methods, and found that CDNVs contained CuB and exhibited superior cytotoxicity to free CuB. We explored the mechanism of the anticancer effects of CDNVs, and found that they could suppress the signal transducer and activator of transcription 3 (STAT3) pathway, enhance reactive oxygen species (ROS) generation, promote cell cycle arrest and increase caspase activity. We reasoned that the lipid bilayers of CDNVs are likely to provide CuB with an enclosed environment and thus improves the bioavailability of CuB. Encapsulated CuB may retain its original structure and activity as it travels through the circulatory system to target cells and initiate cell apoptosis pathways. We also evaluated the safety and anticancer effects of CDNVs in vivo using BALB/c nude male mice bearing tumors consisting of human lung cancer (A549) cells.

This research provides a new perspective on therapeutic drug isolation from medicinal plants. Nowadays, medicinal plants are increasingly considered as a rich resource of ingredients for drug development. However, extraction and isolation of bioactive compounds are typically inefficient, which is not ideal for large-scale production. For example, isolation of 1 g of Taxol typically requires 2 yew trees.[37] Thus, rather than directly extracting bioactive compounds by complex processing methods, isolation of natural PDNVs that contain them may increase efficiency and efficacy, minimize waste, maximize sustainability, and eventually help to drive the global green economy and satisfy the growing worldwide demand for traditional medicine and ethnomedicine.

Materials and Methods

Materials

Cucumbers were purchased from a local market, and were identified by Prof. Yonghong Zhang (the School of Pharmacy, Fujian Medical University). A voucher specimen (No. CSL-20220118) has been deposited in the Pharmacognosy Laboratory of the School of Pharmacy, Fujian Medical University, Fuzhou, China. CuB, Hoechst stain, and caspase-9 and caspase-3 activity detection kits were obtained from Solarbio Science & Technology Co., Ltd (Beijing, China). Phosphate-buffered

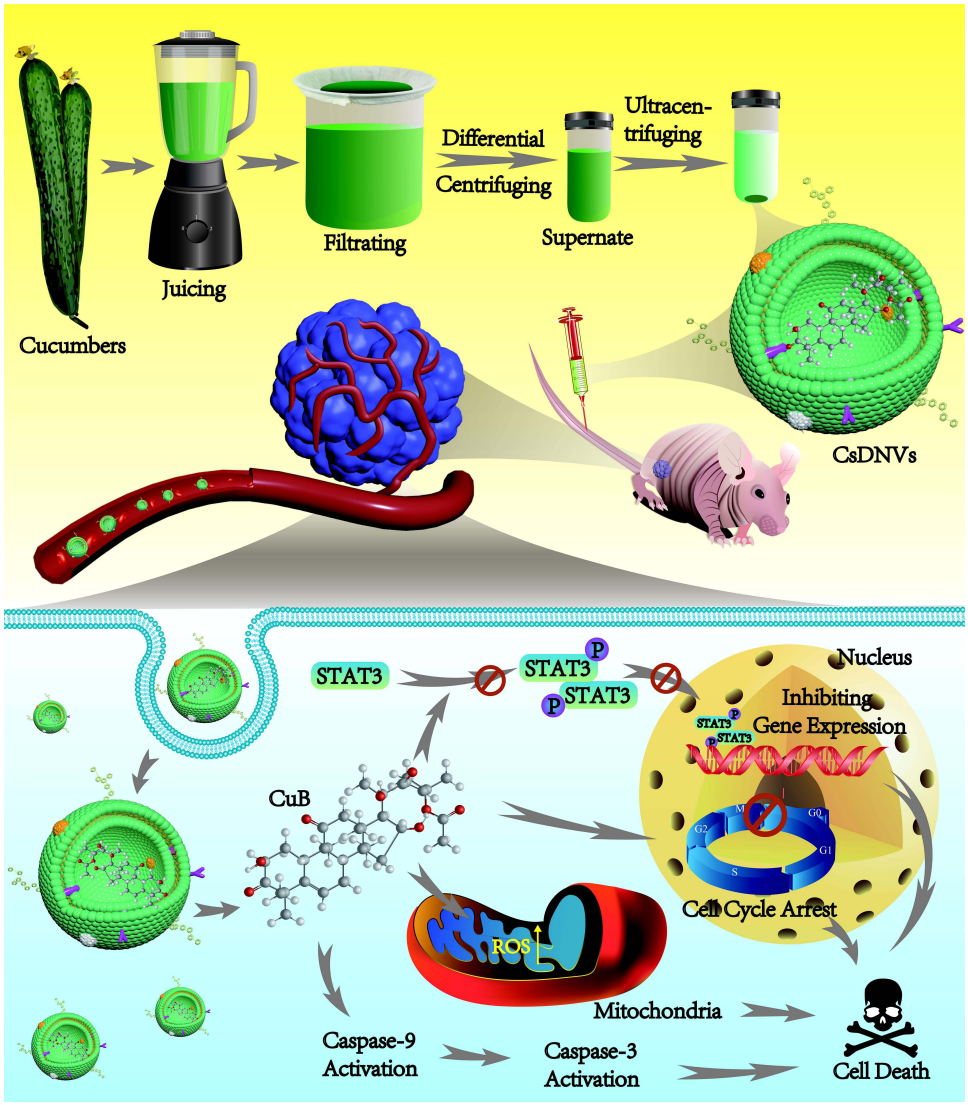

Scheme 1 CsDNVs obtained by juicing and centrifugation were used to inhibit tumor development in nude mice.

saline (PBS), penicillin-streptomycin solution and fetal bovine serum (FBS) were supplied by Hyclone (Shanghai, China). Roswell Park Memorial Institute (RPMI) 1640, Trypsin-EDTA and BCA protein assay kits were purchased from Thermo Fisher Scientific (Shanghai, China). DiO, DiI and ROS assay kits were obtained from Beyotime Biotechnology (Shanghai, China). 3-(4,5-dimethyl-2-thiazolyl)-2,5-diphenyl-2-H-tetrazolium bromide (MTT) was supplied by Sigma-Aldrich (Shanghai, China). Annexin V-FITC/PI apoptosis detection kits and cell cycle detection kits were purchased from Jiangsu KeyGEN BioTECH Corp., Ltd (Nanjing, China). Anti-STAT3 and anti-phosphorylated STAT3 (phospho Y705) antibodies were obtained from Abcam (Shanghai, China). Tumor necrosis factor-α (TNF-α) and interleukin-1β (IL-1β) ELISA kits were purchased from Bioss (Beijing, China).

Cells and Animals

A549 cells were obtained from American Type Culture Collection (ATCC, Shanghai, China). Human gastric carcinoma cells (HGC-27), human hepatocellular carcinoma cells (HepG2) and human breast cancer cells (MDA-MB-231) were obtained from Cell Bank, Chinese Academy of Sciences (Shanghai, China). Cells were cultured in RPMI 1640 containing 10% FBS and 1% penicillin-streptomycin solution under a humidified atmosphere at 5% CO_2 and 37 °C.

Male BALB/c nude mice (6–8 weeks, 16–20 g) were purchased from Shanghai SLAC Laboratory Animal Co., Ltd. (Shanghai, China). Animal studies were performed in accordance with guidelines for the care and use of laboratory animals of Fujian Medical University and approved by the Laboratory Animal Management Committee of Fujian Medical University.

Isolation of CDNVs

CDNVs, including cucumber sarcocarp-derived nanovesicles (CsDNVs) and cucumber pericarp-derived nanovesicles (CpDNVs) were obtained by juicing and ultracentrifugation. Briefly, the cucumbers were thoroughly washed with deionized water. Then the sarcocarp and pericarp were separated and ground into juice in PBS by a blender. The juice was then filtered through gauze to remove large fibers. Residual cells, fibers and large vesicles were removed by centrifuging the filtrate at 5000 × g for 10 min and 10,000 × g for 35 min using a high-speed centrifuge (Heal Force Development Ltd. Neofuge 23R, HongKong). Finally, the supernatant was ultracentrifuged at 30,000 × g for 30 min using an ultracentrifuge (Hitachi, CP100NX, Japan) to obtain CDNV pellets, which were resuspended in PBS for later use.

Characterization of CDNVs

CDNV morphology was observed by transmission electron microscope (TEM, FEI, Tecnai G2), diameter was measured by nanoparticle tracking analysis (NTA), and zeta potential was measured by a laser particle size analyzer (LPSA). To prepare TEM grids, a drop containing CDNVs was fixed with 4% paraformaldehyde (PFA) and then covered by a 200-mesh copper grid. After 20 min, the copper grid was removed and treated with a drop of 2% uranyl acetate for another 5 min to negatively stain the CDNVs. The grids were then dried at room temperature for TEM imaging.

CuB Analysis

High performance liquid chromatography (HPLC) was used to determine the retention times of CuB and CDNV extracts. The extraction process can be briefly described as follows: CDNV pellets were resuspended in methanol and ultrasonicated for 15 min. The solution was then centrifuged and the supernatant was collected; the precipitate was resuspended in methanol and again ultrasonicated and centrifuged. This process was repeated twice, and all supernatants were collected and combined. Before analysis, the supernatant was filtered through 0.22 μm filters. For analysis, the mobile phase consisted of 45% acetonitrile and 55% distilled water, and the detection wavelength was 228 nm. The content was analyzed at 30 °C using a flow velocity of 1 mL/min.

Liquid Chromatography Mass Spectrometry (LC-MS) was used to determine the contents of the CDNVs. Firstly, full scan mode and multiple reaction monitoring (MRM) mode were used to confirm the parent and daughter ions of CuB. Then CDNV extract was scanned in MRM mode to investigate whether it contained the same daughter ion as CuB.

Cellular Uptake of CDNVs

In the cellular uptake assay, A549 cells were seeded into glass-bottomed cell culture dishes at a concentration of 2×10^5 cells/dish and cultured at 37 °C overnight. Then CDNVs were labeled with a green fluorescent lipophilic dye, DiO, for 30 min at 37 °C, followed by washing twice with PBS. Subsequently, A549 cells were incubated with DiO-labeled CDNVs for 1, 4 and 8 h at 37 °C. The A549 cells were then stained by a red cell-membrane dye, DiI, for 15 min and fixed with 4% PFA for 20 min. Finally, Hoechst 33,258 was used to stain the A549 cell nuclei for 15 min. Cells were observed under a confocal laser scanning microscope (Leica, TCS SP, Germany).

Cell Viability

Cell viability was determined by the MTT assay. A549, HGC-27, HepG2 and MDA-MB-231 cells were seeded into 96-well plates at a density of 10,000 cells/well. After 24 h co-incubation with a range of concentrations of free CuB or CDNVs, the cells were treated with 100 μL MTT at 37 °C for 4 h, and 150 μL dimethylsulfoxide was then added to dissolve the formazan for absorbance measurements at 570 nm using a microplate analyzer (BioTek Instruments).

Apoptosis Assay

A549 cells were incubated with 10 nM CuB, CDNVs containing 10 nM CuB, or PBS alone for 24 h, and then collected and washed twice with PBS. Subsequently, 500 μL binding buffer supplied with the Annexin V-FITC/PI apoptosis detection kit was used to resuspend the cells. Then 5 μL AnnexinV-FITC and 5 μL propidium iodide (PI) were added to cells in sequence and incubated at room temperature for 15 min in the dark. Finally, the treated cells were analyzed by flow cytometry (Becton, Dickinson and Company, FACSVerse).

Western Blotting (WB)

WB was used to assess expression of STAT3 and phosphorylated STAT3 (p-STAT3) in A549 cells before and after incubation with free CuB (0, 0.01, 0.1, 1 and 10 nM) and CsDNVs (containing 0, 0.044, 0.089, 0.177 and 0.354 nM CuB) for 24 h. Briefly, treated cells were collected and lysed by radioimmunoprecipitation assay lysis buffer containing 1% phenylmethylsulfonyl fluoride and 1% phosphatase inhibitors on ice for 30 min, then centrifuged at 12,000 rpm for 10 min to obtain the protein supernatant. After heat denaturation, proteins were separated by SDS-polyacrylamide gel electrophoresis (SDS-PAGE) and transferred to polyvinylidene fluoride (PVDF) membranes. Subsequently, 5% skim milk was used to block the PVDF membranes for 2 h. After washing by TBS (tris-buffered saline) and TBST (tris-buffered saline + Tween 20), PVDF membranes were incubated with STAT3, p-STAT3 or β-actin primary antibody followed by a secondary antibody. Finally, protein expression was measured by covering the PVDF membranes with developing solution in a WB imaging system, and the relative intensity of protein band was analyzed by Image Lab software.

Cell Cycle Assay

A549 cells were treated with CsDNVs (protein concentration was 0.17 μg/mL) and PBS (control group). In accordance with the cell cycle detection kit protocol, the treated cells were collected and fixed with pre-cooled 70% ethanol at 4 °C overnight. Subsequently, the fixed cells were centrifuged to remove the ethanol and washed twice with PBS, after which they were immersed in pre-prepared PI/RNaseA solution and incubated for 30 min in the dark at room temperature for cell cycle analysis by flow cytometry.

ROS Detection

A549 cells were treated with PBS, Rosup, CuB and CsDNVs for 4 h. After washing by FBS-free RPMI 1640 for 3 times, A549 cells were incubated with DCFH-DA for 20 min. Finally, Hoechst 33,258 was used to stain the A549 cell nuclei for 20 min. Cells were observed under an inverted fluorescence microscope (Leica, DMI3000 B, Germany).

Caspase-9 and Caspase-3 Activity Assay

After treatment with CsDNVs (protein concentration was 0.17 μg/mL) for 24 h, A549 cells were collected by centrifugation at 1000 rpm for 5 min. In accordance with the caspase-3 and caspase-9 activity detection kit protocols, cells were lysed in 100 μL reagent II on ice for 15 min, and then centrifuged at 15,000 × g for 15 min to obtain the supernatant, of which 50 μL was further incubated with 40 μL reagent I and 10 μL reagent III at 37 °C. Subsequently, the absorbance of the above mixture was measured at 405 nm by a microplate analyzer for calculation of paranitroaniline (pNA) concentration using the pNA standard curve. Finally, the caspase-3 and caspase-9 activities were calculated as follows:

Caspase-3 or caspase-9 activity (U/mg protein) = $2x/C_{pr}/T$, where x represents pNA concentration, C_{pr} represents protein concentration of the sample, and T represents incubation time of the sample in reagents I and III.

Hemolysis Test

Fresh blood was obtained from nude mice and centrifuged at 1000 × g for 5 min to collect red blood cells (RBCs). After washing 3 times with PBS, the RBCs were resuspended in PBS to a concentration of 2%. Subsequently, 2% RBCs were added to equal volumes of PBS, H_2O and CsDNVs (containing 118, 236, 472 nM CuB), respectively. After incubating at

37 °C for 1 h, the mixtures were centrifuged at 10,000 × g for 5 min to obtain the supernatant, the absorbance of which was measured at 541 nm by a microplate reader. The hemolysis ratio was calculated as follows:

$$\text{Hemolysis ratio } (\%)=(A_{CsDNVs}-A_{PBS})/(A_{H_2O}-A_{PBS})\times 100\%$$

Quantitative Measurement of Proinflammatory Cytokines

Mice were randomly divided into 3 groups that were administered 200 μL PBS, 472 nM CuB or CsDNVs containing 472 nM CuB by intravenous injection every day for 7 days. Twenty-four hours after the final treatment, serum of the mice was collected to measure the proinflammatory cytokines. In accordance with the assay protocol, 100 μL standards and serum samples were added to antibody-coated microplates, followed by incubation of 50 μL biotinylated antibody for 120 min to form a sandwich structure. After washing, 100 μL horseradish peroxidase-labeled streptavidin was added to the microwells and incubated at room temperature. After 30 min, the microwells were washed again, and 100 μL chromogenic substrate was added and incubated for 20 min in the dark. Finally, stop buffer was used to terminate the reaction and the solution turned yellow. The TNF-α and IL-1β concentrations were calculated according to the equation for the standard curve of absorbance as a function of concentration.

In-Vivo CsDNV Antitumor Activity Assay

In order to investigate the in-vivo anti-tumor activity of CsDNVs, a lung cancer mouse model was established by subcutaneously inoculating A549 cells (2×10^6 cells) into the left flanks of mice. When the tumor volume reached *ca*. 80 mm^3, mice were randomly divided into 3 groups and respectively administered 200 μL PBS, 472 nM CuB or CsDNVs containing 472 nM CuB by intravenous injection every other day for 14 days. During the treatment period, body weight and tumor volume were recorded every day. After 14 days, mice were sacrificed to remove the solid tumors for photographing and weighing. Then the tumors and major organs (heart, liver, spleen, lung and kidney) were obtained for hematoxylin-eosin (H&E) staining and transferase-mediated deoxyuridine triphosphate nick end labeling (TUNEL) assays.

CsDNV Distribution in vivo

CsDNVs containing 472 nM CuB were incubated with lipophilic DiR dye (100 μM) at 37 °C for 30 min, then centrifuged to discard free dye followed by washing twice with PBS. The pellets were resuspended in PBS to produce the CsDNVs-DiR solution. Subsequently, mice were treated with 200 μL CsDNVs-DiR or an equal amount of free DiR solution by tail vein injection. After 3, 6, 12 and 24 h, the distributions of CsDNVs and free DiR in tumors were observed using a small animal imaging system.

Statistical Analysis

Statistical differences were determined using Student's *t*-test. $P < 0.05$ was used as the minimal level of statistical significance.

Results and Discussion

Isolation and Characterization of CDNVs

CDNVs were isolated by centrifuging juice from cucumbers (CsDNVs from sarcocarp and CpDNVs from pericarp) at 100,000 × g for 60 min followed by a typical exosome isolation protocol. However, the CsDNVs and CpDNVs both severely aggregated (Figure 1A and C), a problem that also exists for other PDNVs isolation protocols when using high centrifugal force for extended durations.[25,38] Thus, to obtain monodisperse CDNVs with intact morphology, the centrifugation parameters were adjusted. We first shortened centrifugal time to 30 min, but the CsDNVs and CpDNVs were still broken, and the aggregation problem just improved slightly (Figure 1B and D). Inspired by PDNVs isolation protocols that use centrifugal forces below 100,000 × g,[39,40] we further optimized centrifugal force and found that the smallest CDNV diameters were obtained using 30,000 × g (Figure 1E and F), suggesting that reducing centrifugal force decreases vesicle aggregation. TEM showed that CsDNVs and CpDNVs isolated under these optimized conditions (30,000 × g, 30 min) were monodisperse and

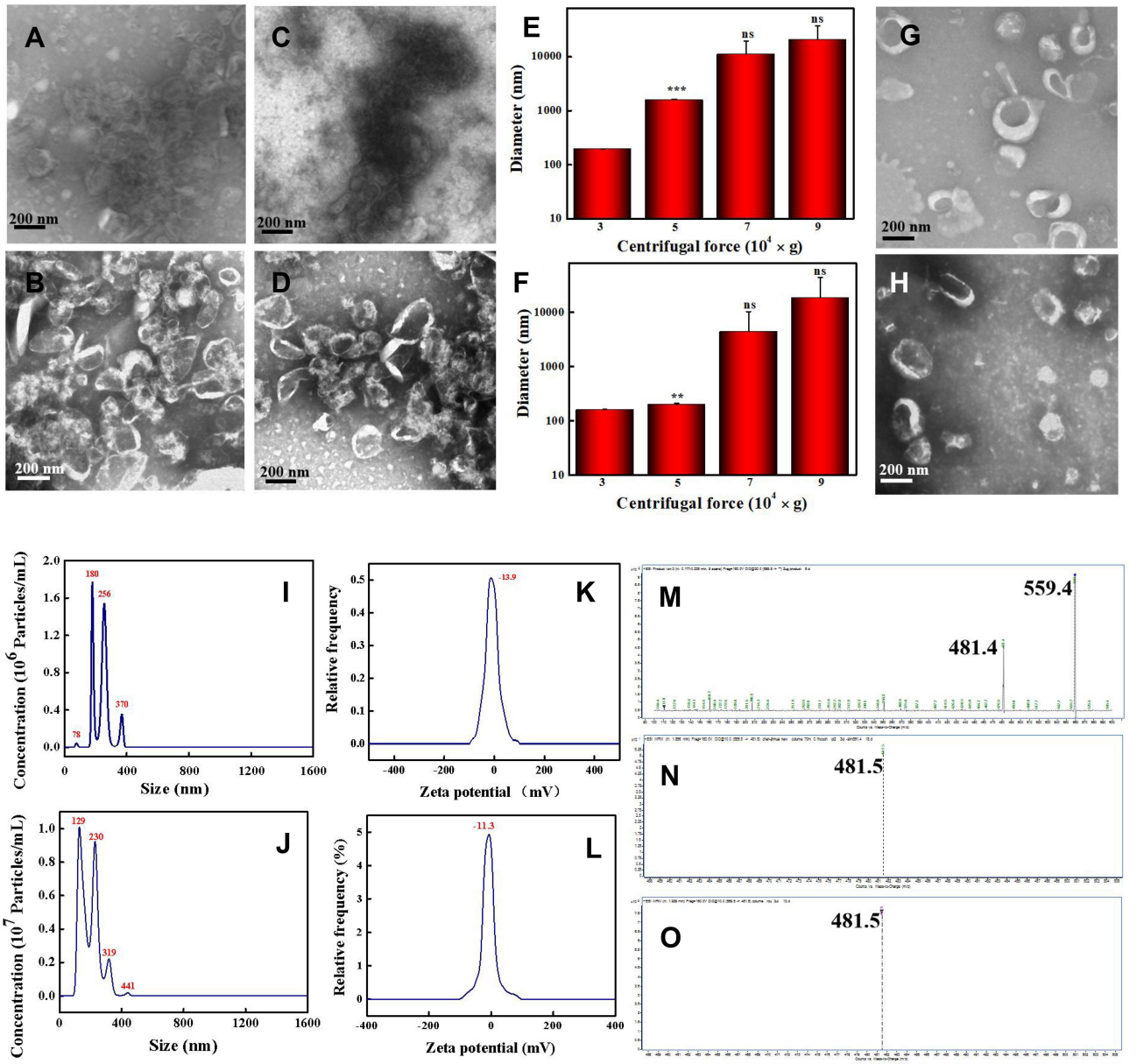

Figure 1 Characterization of Cucumber-derived nanovesicles (CDNVs). (**A** and **B**) TEM images of CsDNVs obtained under a centrifugal force of 100,000 g for 60 min and 30 min, respectively. (**C** and **D**) TEM images of CpDNVs obtained under a centrifugal force of 100,000 g for 60 min and 30 min, respectively. Scale bar: 200 nm. (**E** and **F**) Diameters of CsDNVs and CpDNVs, respectively, obtained under different centrifugal forces. **p < 0.01 vs 30,000 × g group. ***p < 0.001 vs 30,000 × g group. N=3. (**G** and **H**) TEM images of CsDNVs and CpDNVs, respectively, obtained under a centrifugal force of 30,000 g for 30 min. Scale bar: 200 nm. (**I** and **J**) Distribution of diameters of CsDNVs and CpDNVs, respectively, obtained under a centrifugal force of 30,000 g for 30 min. (**K** and **L**) Zeta potentials of CsDNVs and CpDNVs, respectively, obtained under a centrifugal force of 30,000 g for 30 min. (**M**), (**N** and **O**) LC-MS analysis of CuB, CsDNV and CpDNV content, respectively.

exhibited intact saucer-shaped structures (Figure 1G and H), and NTA indicated that the diameters of CsDNVs and CpDNVs were about 180 nm and 129 nm (Figure 1I and J), respectively, consistent with the TEM results. As shown in Figure 1K and L, the zeta potentials of the CsDNVs and CpDNVs were about −13.9 mV and −11.3 mV, respectively. A negative charge is desirable since it prolongs the half-life of CDNVs in the blood circulation.[41] In order to investigate the stability of CDNVs (method details in the supplementary material), we also measured the diameter and PDI change of CDNVs in 10% and 50% FBS solution. As Figure S1 showed in the Supplementary Material, the diameter and PDI of CDNVs did not change much in different concentrations of FBS solution at 37°C in 24 h, indicating that CsDNVs were relatively stable. These results suggested that CDNVs obtained under 30,000 × g centrifugal force for 30 min were structurally intact, well dispersed, stable, and had a diameter and electric potential suitable for in-vivo delivery to tumor tissues.

HPLC and LC-MS for CuB Analysis

Cucumbers not only contain large quantities of beneficial nutrients, but also have phytochemical and therapeutic potential that may help treat and even prevent some medical conditions, and are considered medicinal plants in ethnomedicine such as traditional Mongolian medicine and Dai medicine. Cucumbers are rich in CuB, which many studies have shown to inhibit cancer cell growth.[30–33] Herein, we performed HPLC to identify CuB in CDNVs. As shown in the chromatograms of Figure S2, both CsDNVs and CpDNVs had a peak retention time of 14.7 min, the same as for CuB, indicating that both CsDNVs and CpDNVs contained CuB. These two kinds of CDNVs were further analyzed by LC-MS. The daughter ions m/z 481.5 for both CsDNVs and CpDNVs (Figure 1N and O) were consistent with the daughter ion m/z 481.4 for CuB (Figure 1M), further confirming the presence of CuB in CDNVs. These results demonstrated that CDNVs are a natural nanocarrier of CuB. Without the need of complex encapsulating procedures for CuB in synthetic and artificial nanocarriers,[35,36] CDNVs serve as both a nanocarrier and a resource of CuB to improve the bioavailability and thereby a better anticancer effect of CuB without the risk of the potential toxicity from engineered nanoparticles.

Cellular Uptake of CDNVs

To investigate delivery of CuB to cancer cells via CDNVs, we analyzed uptake of CDNVs by A549 cells using confocal laser scanning microscope. As shown in Figures 2A and S3A, DiO-labeled CsDNVs and CpDNVs were effectively internalized by A549 cells. In addition, as incubation time increased, fluorescence in the A549 cells gradually increased (Figures 2B and S3B), suggesting that CDNVs are taken up by A549 cells in a time-dependent manner. To investigate whether CuB enter the cells with CDNVs (method details in the supplementary material), A549 cells incubated with CDNVs were lysed for LC-MS analysis. As Figure S4 shown, CuB daughter m/z ion was detected at the same retention time (2.0 min, MRM) in CuB standard solution, lysis solution of CsDNVs and CpDNVs treated cells, respectively, demonstrating that CuB did enter the cells with CDNVs.

Anticancer Effects of CDNVs in vitro

The anticancer effects of CDNVs in vitro were assessed by the MTT assay. As shown in Figure 2C, cell viability gradually decreased as CuB concentration increased. CsDNVs and CpDNVs caused significant cytotoxicity toward A549 cells with a 50% inhibitory concentration (IC_{50}) of 4.82 nM and 6.71 nM, respectively (Table S1), while the IC_{50} value of CuB for A549 cells was 95.51 nM, similar to that of a previous study.[34] Chromatin condensation in A549 cells was clearly observed after treatment with CsDNVs or CpDNVs, both of which contain 20 nM CuB. Little chromatin condensation occurred in A549 cells after treatment with 20 nM free CuB (Figure S5), suggesting that CDNVs that contain CuB possess higher anticancer potency than does free CuB. The annexin V-FITC/PI assay was used to further evaluate the cytotoxicity of CuB and CDNVs toward A549 cells. As shown in Figure 2D and E, after treatment with equivalent concentrations of CuB, the percentage of apoptotic cells treated with free CuB was the lowest, CpDNVs higher, and CsDNVs the highest, consistent with the MTT results. These results suggest that the superior cytotoxicity of CDNVs may benefit from the structure of nanovesicles, as they not only protect CuB from the influence of complex external environment factors, but also promote the uptake of CuB by A549 cells.

In order to investigate whether other PDNVs have stronger cytotoxicity to A549 cells, we isolated aloe and Stachys geobombycis derived nanovesicles, and explore their cytotoxicity by MTT assay (method details in the supplementary material). As shown in Figure S6, aloe derived nanovesicles exhibited weak cytotoxicity, and Stachys geobombycis derived nanovesicles had no cytotoxicity to A549 cells. In addition, we also compared the cytotoxicity of CsDNVs to other plant-derived materials and clinically available drugs in other research papers.[27,42–45] Garlic derived nanovesicles were also found having cytotoxicity to A549 cells,[27] but they only inhibited ca. 65% of the cell viability which was lower than CsDNVs. In comparison to clinical available drugs, such as DOX, 5-fluorouracil, cisplatin and taxol, CsDNVs also exhibit better cytotoxicity than 5-fluorouracil and cisplatin.[42–45] Although the cytotoxicity of DOX and taxol are similar to CsDNVs, long-term use of DOX can induce cell resistance,[42] resulting in a low efficacy to cancer therapy. Taxol is extracted from yew trees which are natural rare plants, so it is detrimental to the environment and may increase patients'

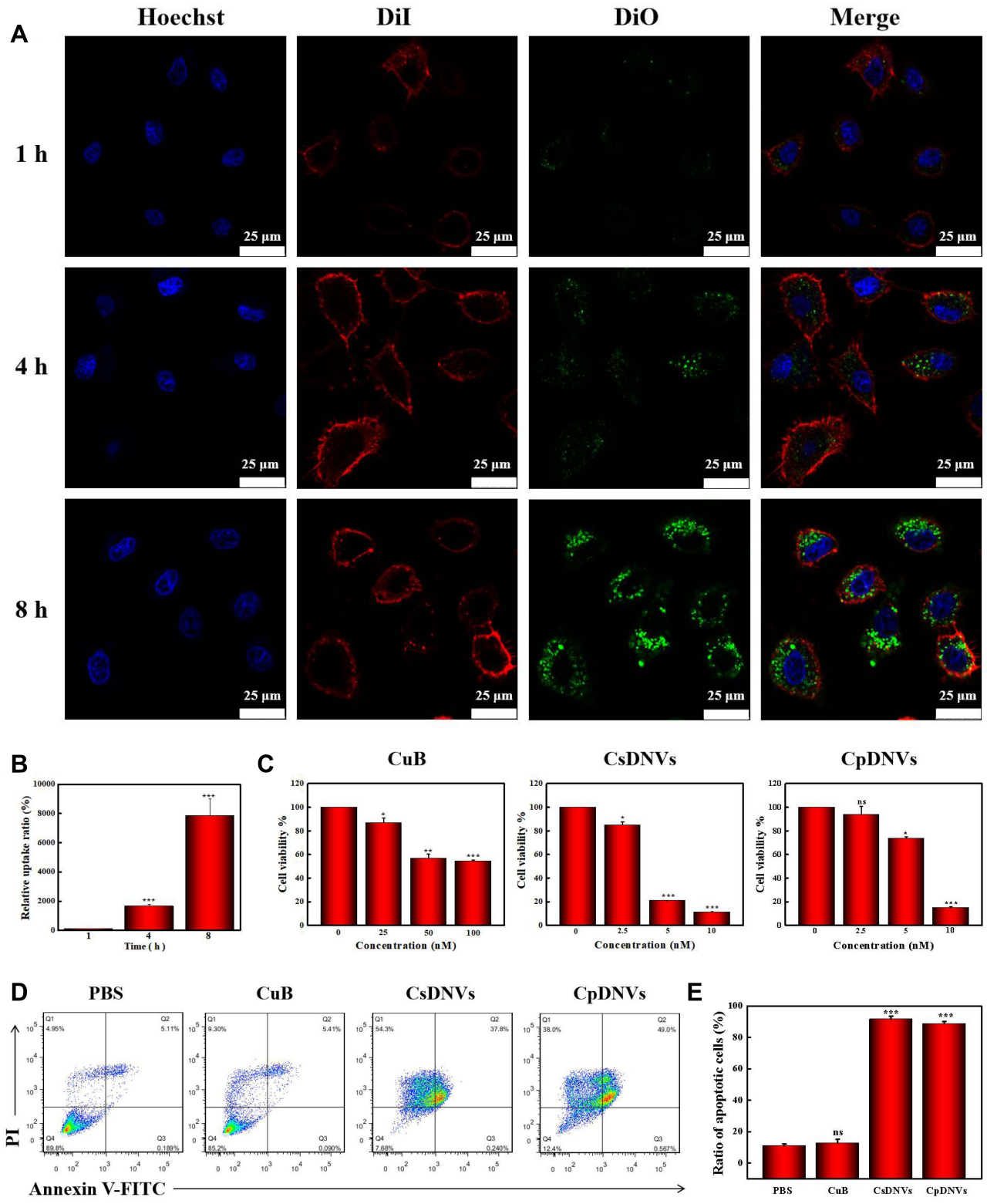

Figure 2 CDNV anticancer properties in vitro. (**A**) A confocal laser scanning microscope was used to observe cellular uptake of CsDNVs. Nuclei were stained with Hoechst, cell membranes were stained with DiI, and CsDNVs were stained with DiO. Scale bar: 25 μm. (**B**) Quantification of the relative uptake ratio of A549 cells to CsDNVs. ***p < 0.001 vs 1 h group. N=3. (**C**) Cytotoxicity of CuB, CsDNVs or CpDNVs was analyzed by the MTT assay. *p < 0.05, **p < 0.01, ***p < 0.001 vs control group. N=3. (**D**) Apoptosis of A549 cells treated by free CuB, CsDNVs or CpDNVs was measured by flow cytometry. (**E**) The ratio of apoptotic cells after treated with free CuB, CsDNVs or CpDNVs. ***p < 0.001 vs PBS group. N=3.

https://doi.org/10.2147/IJN.S362244 DovePress

economic burden.[45] Considering the high anticancer efficacy, anti-resistance potential, and low production cost, CsDNVs may be a more satisfactory drug for clinical lung cancer therapy.

Additional cancer cell lines, including HepG2 cells, MDA-MB-231 cells and HGC-27 cells, were used to evaluate the anticancer effects of CDNVs. As shown in Figure S7, both CsDNVs and CpDNVs have cytotoxicity to all the investigated cancer cell lines in a dose-dependent manner, suggesting potent cytotoxicity. As shown in Table S1, the IC_{50} values of CDNVs for these cancer cells were all below 10 nM. Bakar-Ates et al and Tang et al used lipid polymer hybrids and micelles to load CuB, which resulted in enhanced cytotoxicity toward MDA-MB-231 and HepG2 cells, respectively.[35,36] However, the IC_{50} values of CDNVs in our study were even lower than theirs (14.75 μM for a CuB-lipid polymer hybrid with MDA-MB-231 cells and 76.95 nM for CuB-micelles with HepG-2 cells), suggesting that anticancer efficacy of CuB may be greater with CDNVs than artificially prepared vesicles. Furthermore, unlike CuB-lipid polymer hybrids and CuB-micelles that require extra CuB extraction and loading steps, simpler preparation makes production of CDNVs more feasible for mass manufacture.

Given that CsDNVs inhibited cell viability to a greater extent than did CpDNVs, we only investigated CsDNVs in the following experiments.

The Mechanism of the Anticancer Effects of CsDNVs

STAT3 mediates diverse cellular processes, including proliferation,[46] metastasis,[47] differentiation,[48] and angiogenesis.[49] While STAT3 activation is strictly controlled in healthy cells, STAT3 is constitutively activated by phosphorylation in various types of cancers, where it dimerizes and enters the nucleus to bind to specific genes to promote transcription.[50] Suppression of STAT3 activation has emerged as a promising therapeutic strategy for numerous cancers. There is evidence that CuB-induced cell apoptosis involves the STAT3 pathway.[51,52] Thus, to further investigate the superior anticancer efficacy of CsDNVs compared with free CuB, the levels of STAT3 and p-STAT3 in A549 cells treated with free CuB or CsDNVs were measured by WB. Given that tyrosine phosphorylation of STAT3 is essential for the Janus kinase STAT3 (JAK-STAT3) pathway, which is the canonical pathway for STAT3 activation, primary antibody targeting to phosphorylated tyrosine-705 (pY705) was utilized here to detect p-STAT3. As shown in Figure 3A–C, A549 cells treated with CsDNVs expressed less p-STAT3 in a concentration-dependent manner, while the total level of STAT3 protein was unaffected. This result suggests that CsDNVs inhibited p-STAT3 levels, mainly by suppressing STAT3 phosphorylation rather than decreasing total STAT3 expression. The effects of CuB on STAT3 phosphorylation were similar to those of CsDNVs (Figure 3D–F), consistent with previous research.[32] Interestingly, CsDNVs containing less CuB (0.354 nM) reduced the relative intensity of the p-STAT3 WB band more than did free CuB (10 nM). We believe it may be the serum albumin in FBS that affected free CuB suppressing the STAT3 phosphorylation. Serum albumin can bind to free CuB to form a dimer before CuB is internalized by cells since the binding constant of CuB to serum albumin is relatively high.[53] Dimerization of CuB might reduce binding of CuB to STAT3, thereby reducing its effect on suppression of STAT3 activation.[51] However, the lipid bilayers of CsDNVs can separate CuB from serum albumin, allowing the CuB within CsDNVs to inhibit STAT3 phosphorylation at lower concentrations. Since STAT3 mediates metastasis, we also investigate the CsDNV anti-metastasis efficacy to A549 cells (method details in the supplementary material). As shown in Figure S8A and B, CsDNVs can inhibit cell metastasis. It is worth noting that CuB-mediated suppression of STAT3 phosphorylation is associated with reduced cell resistance to drugs,[54] thus CsDNVs may increase cancer cell sensitivity to some drugs to enhance their anticancer efficacy.

Next, the mechanism of CsDNV inhibition of A549 cell proliferation was further explored. Several cellular processes, including proliferation, differentiation, senescence, and apoptosis, are intimately linked to cell cycle regulation. Abnormal differentiation and growth of malignant tumors are generally associated with cell cycle dysregulation, and cell apoptosis is usually associated with cell cycle arrest. Therefore, the distribution of CsDNV-treated A549 cells within the cell cycle was analyzed. As shown in Figure 3G and H, treatment with CsDNVs (protein concentration, 0.17 μg/mL) resulted in an increase in the percentage of cells in G2/M phase from 4.4% to 8.61%, suggesting that CsDNVs could induce cell cycle arrest in G2/M phase.

An increase in the levels of ROS is believed to inhibit tumor growth and promote apoptosis. It has also been reported that ROS can induce gasdermin D (GSDMD) oligomerization and increase membrane pore formation, further leading to

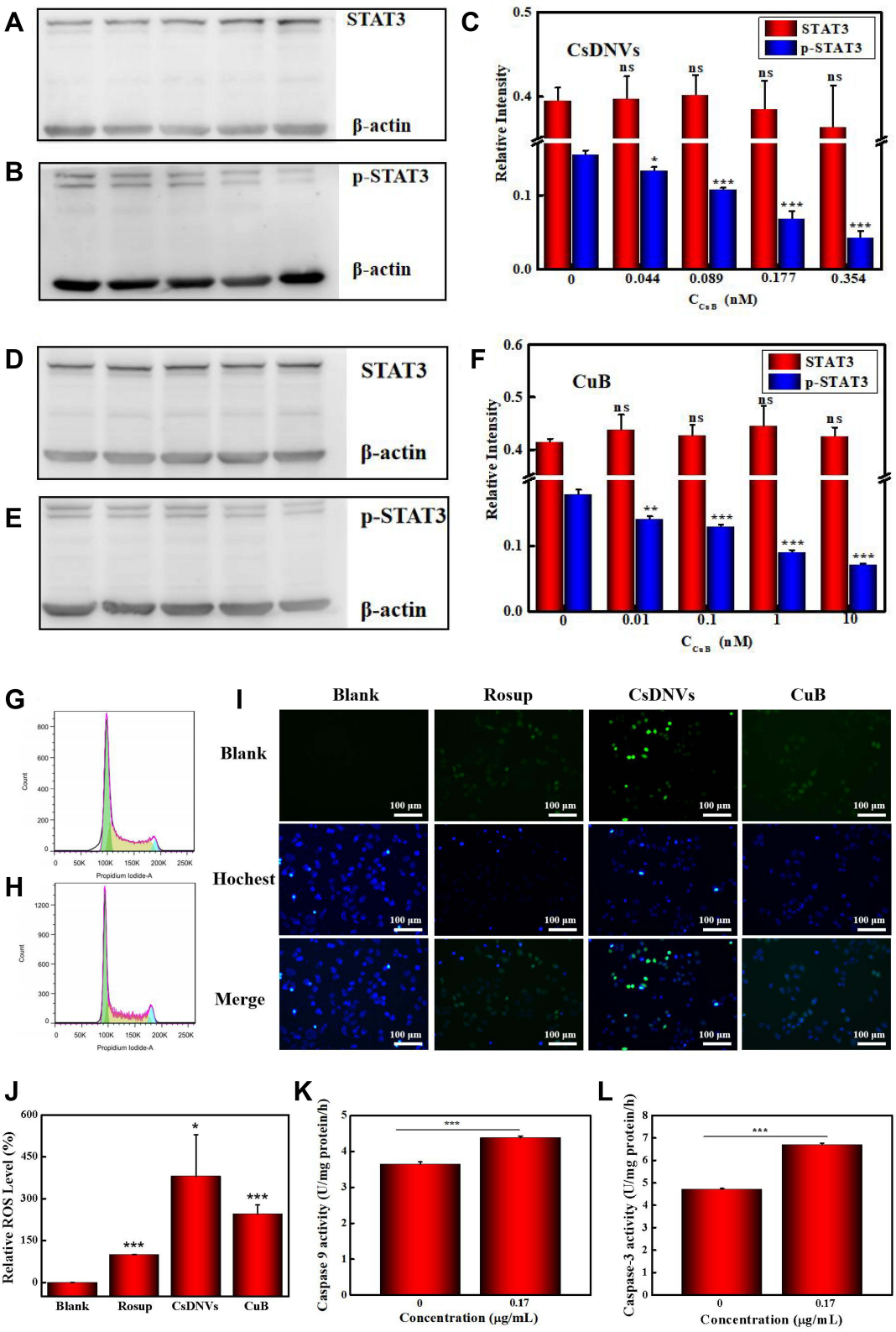

Figure 3 Mechanism of the anticancer effects of CsDNVs. (**A**) STAT3 and (**B**) p-STAT3 expression in A549 cells treated with CsDNVs was analyzed by WB. (**C**) Relative protein levels of STAT3 and p-STAT3 in A549 cells treated with CsDNVs were analyzed by Image Lab software. *p < 0.05, ***p < 0.001 vs control group. N=3. (**D**) STAT3 and (**E**) p-STAT3 expression level of A549 cells treated with CuB was analyzed by WB. (**F**) The relative protein level of STAT3 and p-STAT3 in A549 cells treated with CuB was analyzed by Image Lab software. **p < 0.01, ***p < 0.001 vs control group. N=3. The cell cycle distribution of A549 cells treated with (**G**) PBS and (**H**) CsDNVs was analyzed by flow cytometry. (**I**) Intracellular ROS levels in A549 cells treated with CuB or CsDNVs were observed by fluorescence microscopy. Scale bar: 100 μm. (**J**) Quantification of ROS level in A549 cells. *p < 0.05, ***p < 0.001 vs Blank group. N=3. (**K**) Caspase-9 and (**L**) caspase-3 activities of A549 cells treated with PBS or CsDNVs were measured by a microplate reader. ***p < 0.001. N=3.

pyroptosis, which has recently received more and more attention in the field of cancer therapy.[55] We therefore investigated ROS generation in CsDNV-treated A549 cells. As shown in Figure 3I and J, both CsDNV-treated and CuB-treated cells were obviously fluorescent, similar to the positive control group (Rosup-treated), whereas cells in the negative control group (PBS-treated) were less fluorescent. These results suggest that CsDNVs can stimulate production of ROS.

Excess ROS can also destroy the mitochondrial membrane, releasing cytochrome C into the cytoplasm. The released cytochrome C further combines with apoptotic protein-activating factor 1 (Apaf-1) to recruit and activate pro-caspase 9 to initiate the caspase cascade (a group of proteases involved in eukaryotic apoptosis).[56] Since CsDNVs could stimulate ROS generation, we also measured caspase-9 activity in A549 cells after CsDNV treatment. As shown in Figure 3K, caspase-9 activity increased from 3.64 to 4.37 U/mg protein/h upon treatment with CsDNVs (protein concentration, 0.17 μg/mL). Caspase-9 can further initiate caspase-3 activity. As shown in Figure 3L, after treating with CsDNVs (protein concentration, 0.17 μg/mL), caspase-3 activity increased from 4.71 to 6.70 U/mg protein/h. It is well known that caspase-3 can degrade structural and functional proteins in cells, ultimately leading to cell apoptosis, and it has been reported that CuB can improve caspase-9 and −3 activities.[32] We therefore suggest that CsDNVs might also promote cell apoptosis through activation of caspase.

In summary, we conclude that CsDNVs may exert anticancer effects via the four pathways shown in Scheme 1. First, CsDNVs can suppress STAT3 phosphorylation, further inhibiting gene expression. Second, CsDNVs can induce A549 cell cycle arrest in G2/M phase and hinder cell division. Third, CsDNVs can increase ROS generation, which destroys DNA and decreases cell survival. And fourth, CsDNVs can increase caspase-9 and caspase-3 activities to degrade structural and functional proteins. Admittedly, more research is needed to explore other potential mechanisms.

Safety of CsDNVs

Hemolysis tests, measurements of proinflammatory cytokines, and H&E staining were used to evaluate the safety of CsDNVs.

The hemolysis test results are shown in Figure 4A. RBCs (2%) were incubated with different concentrations of CsDNVs, and no internal hemoglobin release was observed. The corresponding hemolysis ratios of the CsDNVs measured with a microplate reader were all below 5% (Figure 4B), indicating that CsDNVs injected intravenously do not destroy erythrocytes. In addition, levels of proinflammatory cytokines, including TNF-α and IL-1β, were measured in mouse serum (Figure 4C and D). The results showed that differences in the levels of serum proinflammatory cytokines in these two treatment groups (PBS and CsDNVs) were not statistically significant ($p > 0.05$). To further evaluate the safety of CsDNVs, H&E-stained organ sections from mice administered PBS or CsDNVs were analyzed by microscopy. There was negligible damage observed in organ sections from mice in these two treatment groups (Figure 4E): cardiac muscle fibers appeared complete in sectioned heart muscle, no obvious inflammation was observed in liver sections, few granulocytes were observed in spleen sections, the thickness of alveolar walls did not change significantly in lung sections, and little tubular vacuolization was observed in kidney sections. Taken together, these data show that CsDNVs are nontoxic in vivo, which alleviates safety concerns about the use of CsDNVs in mouse tumor therapy.

The Anticancer Effects of CsDNVs in vivo

To investigate the anticancer effects of CsDNVs in vivo, we explored their efficacy in BALB/c nude male mice bearing tumors composed of A549 cells. The time intervals of CsDNVs and CuB treatment regimen was shown in Figure 5A. As shown in Figure 5B, tumors in mice from the CsDNV group grew more slowly than those from the PBS group ($p < 0.05$), whereas the growth rate of tumors in mice administered free CuB was not significantly different from that in the PBS group ($p > 0.05$). Regardless of the different growth rates of tumors in mice from these three groups, there were no statistically significant differences in body weight ($p > 0.05$) (Figure 5C).

Mice were sacrificed on day 14 to measure tumor weight and size (Figure 5D and E). Tumor weight was lowest in the CsDNV group, while the difference in average tumor weight between the free CuB and PBS groups was insignificant. In Figure 5E, tumors in the CsDNV group were also the smallest, consistent with the tumor growth curve. Histological analysis was used to further evaluate CsDNV treatment efficacy (Figure 5F). H&E staining of tumor sections revealed that tumors in the PBS group exhibited nearly no damage, while tumors from the group treated with free CuB showed

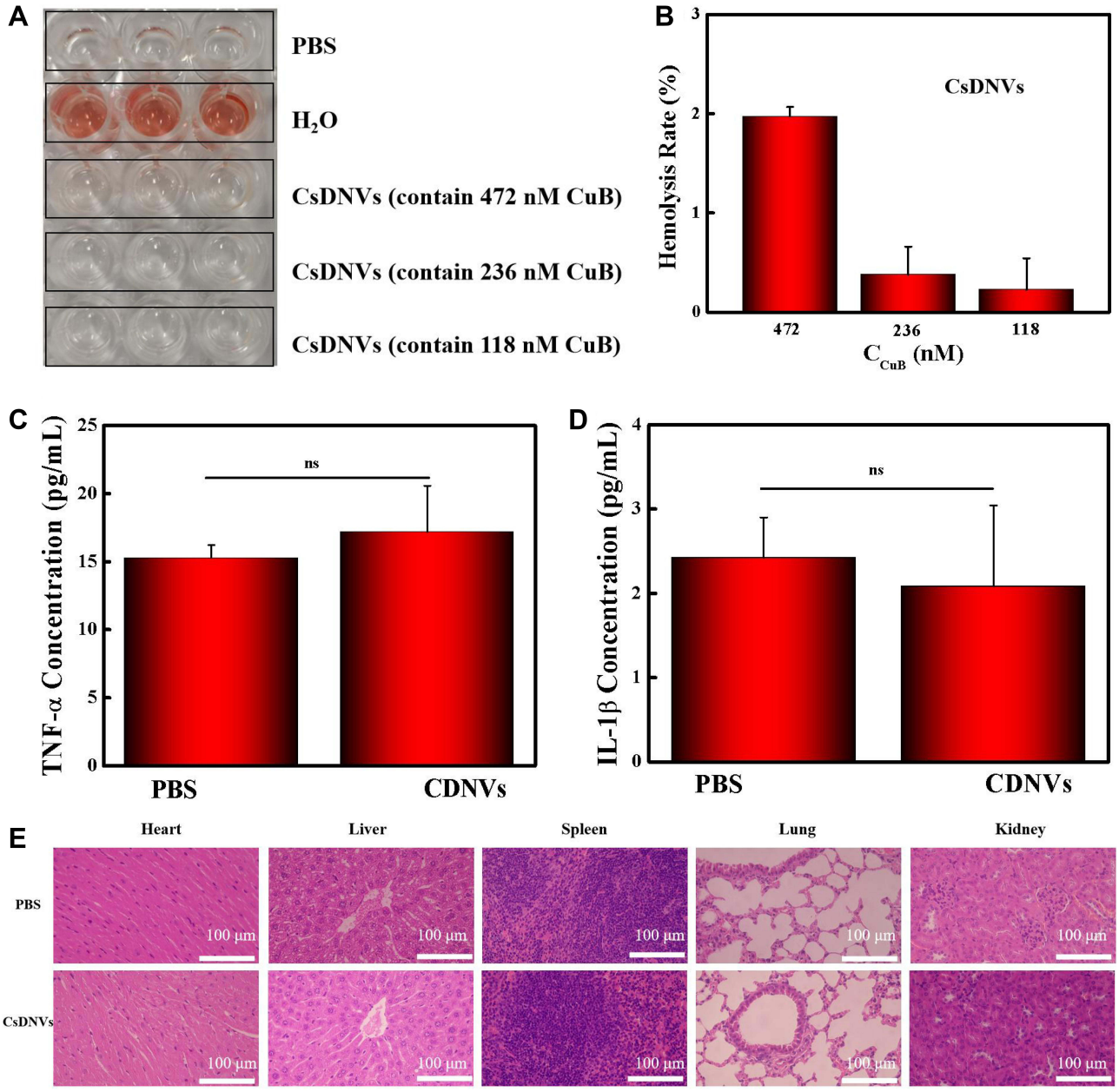

Figure 4 Safety of CsDNVs. (**A**) Hemolysis of CsDNVs was assayed by incubating them with red blood cells. After 1 h, supernatant was decanted for imaging. (**B**) Hemolysis ratios of CsDNVs at different concentrations. N=3. (**C**) TNF-α and (**D**) IL-1β concentration in serum obtained from mice treated daily with PBS and CsDNVs for 7 days. N=3. (**E**) H&E staining of major organs from the different treatment groups. Scale bar: 100 μm.

only slight necrosis. However, after treatment with CsDNVs, tumors exhibited prominent necrosis. The results of the TUNEL assay are shown in Figure S9A and B. Apoptotic cells were observed in tumor sections from mice treated with CsDNVs, but not in the free CuB or PBS groups. These data suggest that CsDNVs possess greater anticancer activity than does free CuB in vivo. In order to investigate whether CsDNVs can inhibit STAT3 activation in vivo (method details in the supplementary material), the level of STAT3 and p-STAT3 in mouse tumor tissues treated with CsDNVs and free CuB have been detected by immunohistochemistry technique, and the related results were shown in Figure S10A and B. The relative expression level of STAT3 and p-STAT3 was quantified in Figure S10C and D, in which we can see that the STAT3 expression level did not change after treated by CuB and CsDNVs. The p-STAT3 expression level decreased after CsDNVs treatment, while it did not change after CuB treatment. These results indicated that CsDNVs can inhibited the

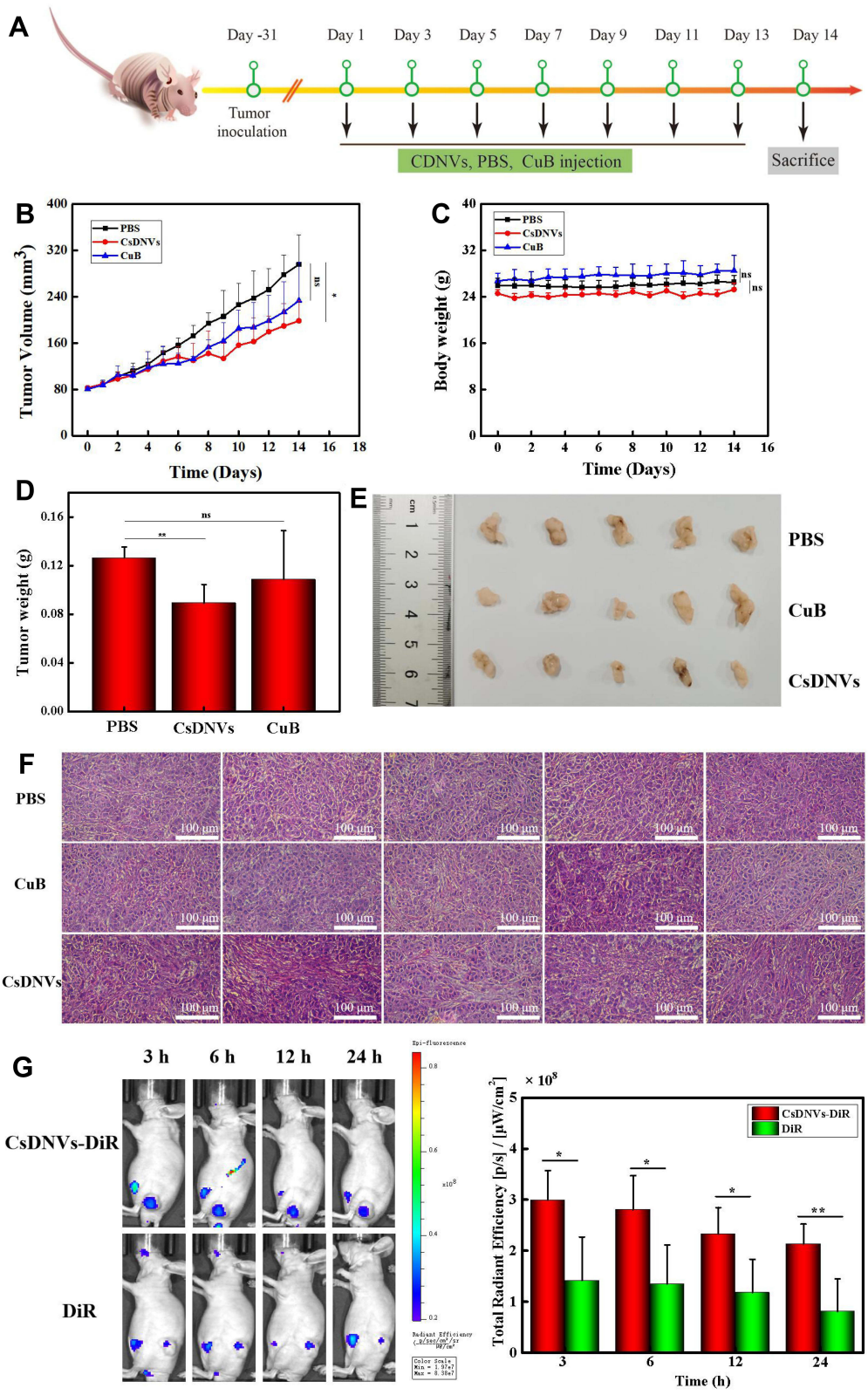

Figure 5 CsDNV anticancer properties in vivo. (**A**) The time intervals of CsDNVs and CuB treatment regimen. (**B**) Tumor volume of nude mice administered PBS, CuB or CsDNVs by tail vein injection. *p < 0.05. N=5. (**C**) Mouse body weight was recorded daily during the treatment period. N=5. (**D**) Tumor weight of nude mice administered PBS, CuB or CsDNVs by tail vein injection. **p < 0.01. N=5. (**E**) Tumor size of nude mice shown after treatment with PBS, CuB or CsDNVs for 14 days. (**F**) H&E staining of tumor tissues from different treatment groups. Scale bar: 100 μm. (**G**) Fluorescence intensity of mice treated with CsDNVs-DiR and free DiR was observed using a small animal live-imaging system. *p < 0.05, **p < 0.01 N=5.

p-STAT3 expression in tumor tissues. Since STAT3 mediate angiogenesis, we also measured the angiogenesis-related factors CD31 expression in tumor tissue from different treatment groups (method details in the supplementary material). As Figure S11A and B shown, CsDNVs can inhibit CD31 expression, which is helpful to inhibiting tumor growing. This may be a result of increased bioavailability of CuB resulting from protection of the nanovesicle structure of CsDNVs, as a previous study reported that the bioavailability of CuB encapsulated by nanocarriers was 1.6 times greater than free CuB, and encapsulated CuB could consequently suppress tumor growth rate more effectively.[36]

Besides increased bioavailability, enhanced permeability and retention may also lead to stronger anticancer effects of CsDNVs. To test this possibility, the biodistribution of CsDNVs in mice was investigated using a small-animal imaging system. DiR, a lipophilic, near-infrared fluorescent cyanine dye used for labeling cytoplasmic membranes, was used to label CsDNVs and track their distribution in vivo. As shown in Figure 5G, the fluorescence intensity of tumors from the DiR-CsDNV group was much stronger than that from the DiR group, demonstrating that CsDNVs could accumulate in tumor tissue, which may contribute to their superior anticancer effects in vivo.

Conclusion

In this research, an in-depth exploration of CsDNVs has been carried out for the first time, and we provide critical evidence demonstrating their anticancer effects. CsDNVs were obtained using a simple method of juicing and ultracentrifugation, and their structure, diameter and zeta potential was similar to mammalian exosomes. We found that these CsDNVs could be taken up by A549 cells where they inhibited proliferation by suppressing STAT3 phosphorylation, enhancing ROS generation, promoting cell cycle arrest and increasing caspase activity. Compared with free CuB, CsDNVs possessed greater anticancer activity, both in vitro and in vivo, which may result from the improved bioavailability of CuB as a result of the protective effect of the lipid bilayer of CsDNVs and accumulation of CuB in tumor tissue via enhanced permeability and retention. In addition to their native therapeutic potential, CsDNVs can also be used to load other agents for synergetic cancer therapy. Other bioactive molecules in CsDNVs may also contribute to inhibition of tumor growth. However, given that CuB widely exists in cucurbitaceous plants, and exhibits anticancer activity in various cancer, we only analyzed CuB in CDNVs in this paper as a simplified study model, and expected it to be a start and a reference for future CDNV research. More studies are required to fully understand the underlying mechanisms of CDNV anti-cancer activity, and to appropriately apply the results to clinical applications. This research provides a novel perspective on therapeutic drug isolation from medicinal plants, which are more likely to be sustainable and help drive the global green economy.

Abbreviations

PDNVs, plant-derived nanovesicles; GDNVs, ginger-derived nanoparticles; GaDNVs, garlic-derived nanovesicles; CuB, cucurbitacin B; CDNVs, cucumber-derived nanovesicles; STAT3, signal transducer and activator of transcription 3; ROS, reactive oxygen species; PBS, phosphate-buffered saline; FBS, fetal bovine serum; RPMI, Roswell Park Memorial Institute; MTT, 3-(4,5-dimethyl-2-thiazolyl)-2,5-diphenyl-2-H-tetrazolium bromide; TNF-α, tumor necrosis factor-α; IL-1β, interleukin-1β; ATCC, American Type Culture Collection; CsDNVs, cucumber sarcocarp-derived nanovesicles; CpDNVs, cucumber pericarp-derived nanovesicles; NTA, nanoparticle tracking analysis; LPSA, laser particle size analyzer; PFA, paraformaldehyde; HPLC, high performance liquid chromatography; LC-MS, liquid chromatography mass spectrometry; MRM, multiple reaction monitoring; PI, propidium iodide; WB, Western blot; p-STAT3, phosphorylated STAT3; SDS-PAGE, SDS-polyacrylamide gel electrophoresis; PVDF, polyvinylidene fluoride; TBS, tris-buffered saline; TBST, tris-buffered saline + Tween 20; pNA, paranitroaniline; RBCs, red blood cells; H&E, hematoxylin and eosin; TUNEL, transferase-mediated deoxyuridine triphosphate nick end labeling; JAK, janus kinase; pY705, phosphorylated tyrosine-705; GSDMD, gasdermin D; Apaf-1, apoptotic protein-activating factor 1.

Acknowledgments

The authors acknowledge financial support from The Innovation of Science and Technology Funding of Fujian province (2019Y9008), Natural Science Foundation of Fujian Province (2020J01545, 2020Y0022). We would like to thank

Zhihong Huang, Cailing Yan, Sishi Chen, Xiuwang Huang, Ling Lin of the Public Technology Center (Fujian Medical University) for their technical assistance.

Disclosure

The authors report no conflicts of interest in this work.

References

1. Ranganathan K, Singh P, Raghavendran K, et al. The global macroeconomic burden of breast cancer: implications for oncologic surgery. *Ann Surg*. 2021;274(6):1067–1072. doi:10.1097/SLA.0000000000003662
2. Murphy N, Campbell PT, Gunter MJ. Are sugar-sweetened beverages contributing to the rising occurrence of colorectal cancer in young adults? *Gut*. 2021;70(12):2222–2223. doi:10.1136/gutjnl-2021-324614
3. Song S, Chen Q, Li Y, et al. Targeting cancer stem cells with a pan-BCL-2 inhibitor in preclinical and clinical settings in patients with gastroesophageal carcinoma. *Gut*. 2021;70(12):2238–2248. doi:10.1136/gutjnl-2020-321175
4. Li S, Lin K, Hu P, et al. A multifunctional nanoamplifier with self-enhanced acidity and hypoxia relief for combined photothermal/photodynamic/starvation therapy. *Int J Pharm*. 2021;611:121307. doi:10.1016/j.ijpharm.2021.121307
5. Chen J, Nie W, Hu Y, et al. A folic acid-modified non-viral vector combines gene therapy with chemotherapy to reverse cancer chemotherapy resistance. *Appl Mater Today*. 2021:101277. doi:10.1016/j.apmt.2021.101277
6. Dai Y, Zhao H, He K, et al. NIR-II excitation phototheranostic nanomedicine for fluorescence/photoacoustic tumor imaging and targeted photothermal-photonic thermodynamic therapy. *Small*. 2021;17(42):e2102527. doi:10.1002/smll.202102527
7. Ding Y, Yang R, Yu W, et al. Chitosan oligosaccharide decorated liposomes combined with TH302 for photodynamic therapy in triple negative breast cancer. *J Nanobiotechnol*. 2021;19(1):147. doi:10.1186/s12951-021-00891-8
8. Nie W, Wu G, Zhang J, et al. Responsive exosome nano-bioconjugates for synergistic cancer therapy. *Angew Chem Int Ed Engl*. 2020;59(5):2018–2022. doi:10.1002/anie.201912524
9. Zhang J, Zhu S, Tan Q, et al. Combination therapy with ropivacaine-loaded liposomes and nutrient deprivation for simultaneous cancer therapy and cancer pain relief. *Theranostics*. 2020;10(11):4885–4899. doi:10.7150/thno.43932
10. Ye WL, Zhao YP, Cheng Y, et al. Bone metastasis target redox-responsive micell for the treatment of lung cancer bone metastasis and anti-bone resorption. *Artif Cells Nanomed Biotechnol*. 2018;46(sup1):380–391. doi:10.1080/21691401.2018.1426007
11. Yang K, Zhang S, He J, et al. Polymers and inorganic nanoparticles: a winning combination towards assembled nanostructures for cancer imaging and therapy. *Nano Today*. 2021;36:101046.
12. Rahman MA, Wang P, Zhao Z, et al. Systemic delivery of Bc12-targeting siRNA by DNA nanoparticles suppresses cancer cell growth. *Angew Chem Int Ed Engl*. 2017;56(50):16023–16027. doi:10.1002/anie.201709485
13. Gregory JV, Kadiyala P, Doherty R, et al. Systemic brain tumor delivery of synthetic protein nanoparticles for glioblastoma therapy. *Nat Commun*. 2020;11(1):5687. doi:10.1038/s41467-020-19225-7
14. Dad HA, Gu TW, Zhu AQ, et al. Plant exosome-like nanovesicles: emerging therapeutics and drug delivery nanoplatforms. *Mol. Ther*. 2021;29(1):13–31. doi:10.1016/j.ymthe.2020.11.030
15. Kim MK, Choi YC, Cho SH, et al. The antioxidant effect of small extracellular vesicles derived from aloe vera peels for wound healing. *Tissue Eng. Regen. Med*. 2021;18(4):561–571. doi:10.1007/s13770-021-00367-8
16. Baldrich P, Rutter BD, Karimi HZ, et al. Plant extracellular vesicles contain diverse small RNA species and are enriched in 10- to 17-nucleotide "tiny" RNAs. *Plant Cell*. 2019;31(2):315–324. doi:10.1105/tpc.18.00872
17. Cai Q, Qiao L, Wang M, et al. Plants send small RNAs in extracellular vesicles to fungal pathogen to silence virulence genes. *Science*. 2018;360(6393):1126–1129. doi:10.1126/science.aar4142
18. You JY, Kang SJ, Rhee WJ. Isolation of cabbage exosome-like nanovesicles and investigation of their biological activities in human cells. *Bioact Mater*. 2021;6(12):4321–4332. doi:10.1016/j.bioactmat.2021.04.023
19. Xia Y, Chen T, Chen W, et al. A dual-modal aptasensor based on a multifunctional acridone derivate for exosomes detection. *Anal Chim Acta*. 2022;1191:339279. doi:10.1016/j.aca.2021.339279
20. Yu L, Deng Z, Liu L, et al. Plant-derived nanovesicles: a novel form of nanomedicine. *Front. Bioeng. Biotechnol*. 2020;8:584391. doi:10.3389/fbioe.2020.584391
21. Ju S, Mu J, Dokland T, et al. Grape exosome-like nanoparticles induce intestinal stem cells and protect mice from DSS-induced colitis. *Mol Ther*. 2013;21(7):1345–1357. doi:10.1038/mt.2013.64
22. Wang Q, Zhuang X, Mu J, et al. Delivery of therapeutic agents by nanoparticles made of grapefruit-derived lipids. *Nat Commun*. 2013;4:1867. doi:10.1038/ncomms2886
23. Teng Y, Ren Y, Sayed M, et al. Plant-derived exosomal microRNAs shape the gut microbiota. *Cell Host Microbe*. 2018;24(5):637–652.e8. doi:10.1016/j.chom.2018.10.001
24. Li Z, Wang H, Yin H, et al. Arrowtail RNA for ligand display on ginger exosome-like nanovesicles to systemic deliver siRNA for cancer suppression. *Sci. Rep*. 2018;8(1):14644. doi:10.1038/s41598-018-32953-7
25. Zhang M, Xiao B, Wang H, et al. Edible ginger-derived nano-lipids loaded with doxorubicin as a novel drug-delivery approach for colon cancer therapy. *Mol Ther*. 2016;24(10):1783–1796. doi:10.1038/mt.2016.159
26. Garaeva L, Kamyshinsky R, Kil Y, et al. Delivery of functional exogenous proteins by plant-derived vesicles to human cells in vitro. *Sci Rep*. 2021;11(1):6489. doi:10.1038/s41598-021-85833-y
27. Özkan İ, Koçak P, Yıldırım M, et al. Garlic (Allium sativum)-derived SEVs inhibit cancer cell proliferation and induce caspase mediated apoptosis. *Sci Rep*. 2021;11(1):14773. doi:10.1038/s41598-021-93876-4
28. Zhang M, Viennois E, Prasad M, et al. Edible ginger-derived nanoparticles: a novel therapeutic approach for the prevention and treatment of inflammatory bowel disease and colitis-associated cancer. *Biomaterials*. 2016;101:321–340. doi:10.1016/j.biomaterials.2016.06.018

29. Yang M, Liu X, Luo Q, et al. An efficient method to isolate lemon derived extracellular vesicles for gastric cancer therapy. *J Nanobiotechnol*. 2020;18(1):100. doi:10.1186/s12951-020-00656-9
30. Ma W, Xiang Y, Yang R, et al. Cucurbitacin B induces inhibitory effects via the CIP2A/PP2A/C-KIT signaling axis in t (8; 21) acute myeloid leukemia. *J Pharmacol Sci*. 2019;139(4):304–310. doi:10.1016/j.jphs.2018.12.010
31. Dittharot K, Dakeng S, Suebsakwong P, et al. Cucurbitacin B induces hypermethylation of oncogenes in breast cancer cells. *Planta Med*. 2019;85 (5):370–378. doi:10.1055/a-0791-1591
32. Zhang M, Bian ZG, Zhang Y, et al. Cucurbitacin B inhibits proliferation and induces apoptosis via STAT3 pathway inhibition in A549 lung cancer cells. *Mol Med Rep*. 2014;10(6):2905–2911. doi:10.3892/mmr.2014.2581
33. Sun Y, Zhang J, Zhou J, et al. Synergistic effect of cucurbitacin B in combination with curcumin via enhancing apoptosis induction and reversing multidrug resistance in human hepatoma cells. *Eur J Pharmacol*. 2015;768:28–40. doi:10.1016/j.ejphar.2015.10.003
34. Yuan R, Zhao W, Wang QQ, et al. Cucurbitacin B inhibits non-small cell lung cancer in vivo and in vitro by triggering TLR4/NLRP3/GSDMD-dependent pyroptosis. *Pharmacol Res*. 2021;170:105748. doi:10.1016/j.phrs.2021.105748
35. Bakar-Ates F, Ozkan E, Sengel-Turk CT. Encapsulation of cucurbitacin B into lipid polymer hybrid nanocarriers induced apoptosis of MDAMB231 cells through PARP cleavage. *Int J Pharm*. 2020;586:119565. doi:10.1016/j.ijpharm.2020.119565
36. Tang L, Fu L, Zhu Z, et al. Modified mixed nanomicelles with collagen peptides enhanced oral absorption of Cucurbitacin B: preparation and evaluation. *Drug Deliv*. 2018;25(1):862–871. doi:10.1080/10717544.2018.1425773
37. Gallego-Jara J, Lozano-Terol G, Sola-Martínez RA, et al. A compressive review about taxol®: history and future challenges. *Molecules*. 2020;25 (24):5986. doi:10.3390/molecules25245986
38. Zhang L, He F, Gao L, et al. Engineering exosome-like nanovesicles derived from asparagus cochinchinensis can inhibit the proliferation of hepatocellular carcinoma cells with better safety profile. *Int J Nanomed*. 2021;16:1575–1586. doi:10.2147/IJN.S293067
39. Woith E, Melzig MF. Extracellular vesicles from fresh and dried plants-simultaneous purification and visualization using gel electrophoresis. *Int J Mol Sci*. 2019;20(2):357. doi:10.3390/ijms20020357
40. Regente M, Corti-Monzón G, Maldonado AM, et al. Vesicular fractions of sunflower apoplastic fluids are associated with potential exosome marker proteins. *FEBS Lett*. 2009;583(20):3363–3366. doi:10.1016/j.febslet.2009.09.041
41. Qin Z, Chen T, Teng W, et al. Mixed-charged zwitterionic polymeric micelles for tumor acidic environment responsive intracellular drug delivery. *Langmuir*. 2019;35(5):1242–1248. doi:10.1021/acs.langmuir.8b00471
42. Dai Z, Song XZ, Cao J, et al. Dual-stimuli-responsive TiO x /DOX nanodrug system for lung cancer synergistic therapy. *RSC Adv*. 2018;8 (39):21975–21984. doi:10.1039/C8RA02899K
43. Tan A, Yaglioglu AS, Kishali NH, et al. Evaluation of cytotoxic potentials of some isoindole-1, 3-dione derivatives on HeLa, C6 and A549 cancer cell lines. *Med Chem*. 2020;16(1):69–77. doi:10.2174/1573406415666181206115638
44. Yang Y, Zhou W, Wu J, et al. Antitumor activity of nimotuzumab in combination with cisplatin in lung cancer cell line A549 in vitro. *Oncol Lett*. 2018;15(4):5280–5284. doi:10.3892/ol.2018.7923
45. Wang C, Chen T. Intratumoral injection of taxol in vivo suppresses A549 tumor showing cytoplasmic vacuolization. *J Cell Biochem*. 2012;113 (4):1397–1406. doi:10.1002/jcb.24012
46. Su Y, Zhang W, Patro C, et al. STAT3 regulates mouse neural progenitor proliferation and differentiation by promoting mitochondrial metabolism. *Front Cell Dev Biol*. 2020;8:362. doi:10.3389/fcell.2020.00362
47. Yang H, Xu W. STAT3 promotes peritoneal metastasis of gastric cancer by enhancing mesothelial-mesenchymal transition. *Biol Chem*. 2021;402 (6):739–748. doi:10.1515/hsz-2021-0120
48. Yang Y, Chung MR, Zhou S, et al. STAT3 controls osteoclast differentiation and bone homeostasis by regulating NFATc1 transcription. *J Biol Chem*. 2019;294(42):15395–15407. doi:10.1074/jbc.RA119.010139
49. Wang Z, Yan M, Li J, et al. Dual functions of STAT3 in LPS-induced angiogenesis of hepatocellular carcinoma. *Biochim. Biophys. Acta Mol. Cell Res*. 2019;1866(4):566–574. doi:10.1016/j.bbamcr.2018.11.016
50. Thilakasiri PS, Dmello RS, Nero TL, et al. Repurposing of drugs as STAT3 inhibitors for cancer therapy. *Semin Cancer Biol*. 2021;68:31–46. doi:10.1016/j.semcancer.2019.09.022
51. Xu J, Chen Y, Yang R, et al. Cucurbitacin B inhibits gastric cancer progression by suppressing STAT3 activity. *Arch Biochem Biophys*. 2020;684:108314. doi:10.1016/j.abb.2020.108314
52. Ding X, Chi J, Yang X, et al. Cucurbitacin B synergistically enhances the apoptosis-inducing effect of arsenic trioxide by inhibiting STAT3 phosphorylation in lymphoma Ramos cells. *Leuk Lymphoma*. 2017;58(10):2439–2451. doi:10.1080/10428194.2017.1289521
53. Abou-Khalil R, Jraij A, Magdalou J, et al. Interaction of cucurbitacins with human serum albumin: thermodynamic characteristics and influence on the binding of site specific ligands. *J. Photochem. Photobiol. B*. 2009;95(3):189–195. doi:10.1016/j.jphotobiol.2009.03.005
54. Ku JM, Kim SR, Hong SH, et al. Cucurbitacin D induces cell cycle arrest and apoptosis by inhibiting STAT3 and NF-κB signaling in doxorubicin-resistant human breast carcinoma (MCF7/ADR) cells. *Mol Cell Biochem*. 2015;409(1–2):33–43. doi:10.1007/s11010-015-2509-9
55. Evavold CL, Hafner-Bratkovič I, Devant P, et al. Control of gasdermin D oligomerization and pyroptosis by the Ragulator-Rag-mTORC1 pathway. *Cell*. 2021;184(17):4495–4511.e19. doi:10.1016/j.cell.2021.06.028
56. Moloney JN, Cotter TG. ROS signalling in the biology of cancer. *Semin Cell Dev Biol*. 2018;80:50–64. doi:10.1016/j.semcdb.2017.05.023